Available online at www.sciencedirect.com
ScienceDirect
Journal of Computational Physics 227 (2008) 5361–5384
JOURNAL OF COMPUTATIONAL PHYSICS
www.elsevier.com/locate/jcp

Reconstruction of multi-material interfaces from moment data

Vadim Dyadechko *, Mikhail Shashkov

Mathematical Modeling and Analysis, Group at the Los Alamos National Laboratory, MS B284, Los Alamos, NM 87545, United States

Received 29 September 2006; received in revised form 12 December 2007; accepted 20 December 2007
Available online 9 February 2008

Abstract

The moment-of-fluid (MoF) method is an extension of popular volume-of-fluid (VoF) technique for tracking material interface in multi-material fluid flows. VoF methods track the cell-wise material volumes and use these data for reconstructing the interfaces in mixed cell. The MoF method goes one step further and, in additional to the volumes, keeps track of the cell-wise material centroids; this approach provides sufficiently more information for the interface reconstruction algorithm.

The MoF algorithm reconstructs interfaces in volume-conservative manner, by minimizing the defect of the 1st moment in each mixed cell. In case of two materials, this strategy allows to construct the linear interface in a mixed cell using no material volume data from the neighboring cells. Compared to the VoF interface reconstruction techniques, the MoF algorithm shows higher accuracy and better resolution, allows uniform processing of internal and boundary cells.

In this paper we show how the same governing principle (minimization of the 1st-moment defect) can be used to reconstruct the interfaces in case of multiple materials.
Published by Elsevier Inc.

Keywords: Multi-material interface reconstruction; Volume-of-fluid method; VoF; Moment-of-fluid method; MoF; Cell-wise material centroids

1. Introduction

Volume-of-fluid (VoF) method is a popular technique for tracking material interfaces in multi-material fluid flows. Originally VoF was developed for Eulerian simulation of incompressible fluid flows with free boundaries [12]. The popularity of VoF methods is due to simple treatment of the interface topology changes and rigorous enforcement of mass conservation of each fluid component. Excellent reviews of the VoF methods and, in particular, interface reconstruction techniques can be found in the following papers [19,7,16,21,20]. We just want to remind some important details.

* Corresponding author.
E-mail address: vdyadechko@gmail.com (V. Dyadechko).

0021-9991/$ - see front matter Published by Elsevier Inc.
doi:10.1016/j.jcp.2007.12.029

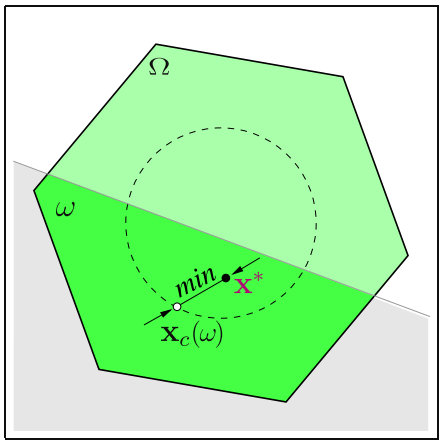

Fig. 1. MoF algorithm for constructing a linear interface in a two-material mixed cell Ω: among all the subcells ω with a linear interface and the prescribed volume, find the one whose centroid $\mathbf{x}_c(\omega)$ is closest to the given centroid $\mathbf{x}^*$. The algorithm uses no data from outside the cell.

On each time step, a typical VoF method:

- updates the material content of the cells, usually by computing fluxes through the cell boundaries,
- reconstructs the material interfaces in the mixed cells from the cell-wise material volumes.

The interface reconstruction is done in volume-conservative manner, which, along with fluxing, guarantees the mass conservation for incompressible fluids. All VoF interface reconstruction algorithms are formulated for two materials, i.e. split a mixed cell into two subcells. The most common interface approximation consists of a single linear interface in each mixed cell. This class of interface reconstructions is commonly called Piecewise-Linear Interface Calculation (PLIC). Since the material volumes are preserved by the reconstruction, the location of the interface is uniquely determined by the direction of the interface normal. There are many different algorithms to derive the interface normal in the VoF context (i.e. from the material volumes for details refer to [8,13,24,22,17,18,14,3,7,16]). All of them rely on the material volume data from the neighboring cells, which prohibits them from resolving small (2–3 cell sizes and less) interface details.

In order to improve the resolution of small details, a new volume-conservative interface tracking method was proposed [9]. The central idea of the *moment-of-fluid* (*MoF*) approach is to supplement the VoF interface reconstruction input data set with the cell-wise material centroids. The material volumes and centroids form a natural input data set for the interface reconstruction, which contains the essential information about the amount and the average location of each material in a mixed cell.

Similar to the VoF, the two-material MoF interface reconstruction algorithm [9] uses linear interface to separate the materials in a mixed cell. The volume and centroid, or, equivalently, the first two moments of the material provide sufficient amount of information to construct such a linear interface *without any data from the adjacent cells*. The direction of the interface normal is determined through minimization of the discrepancy between the actual and the prescribed centroids, subject to matching the prescribed volume exactly (Fig. 1). The results of the MoF reconstruction is *the volume-preserving mixed-cell partition that minimizes the defect of the first moment*. If the true interface is twice-differentiable, the MoF reconstruction is 2nd-order accurate; if the true interface is linear, the reconstruction is exact. The numerical experiments [9] show that the moment-based interface reconstruction demonstrates superior resolution and always results in smaller absolute error, than traditional volume-based techniques.

Since the interface reconstruction is intended for multi-material fluid flow simulations, it is important to have the interface reconstruction input composed of quantities that can be accurately advanced in time. The fact that the material centroids in the incompressible flow move similarly to Lagrangian particles (see Appendix A) makes them a perfect choice for the interface reconstruction input. One can consistently update

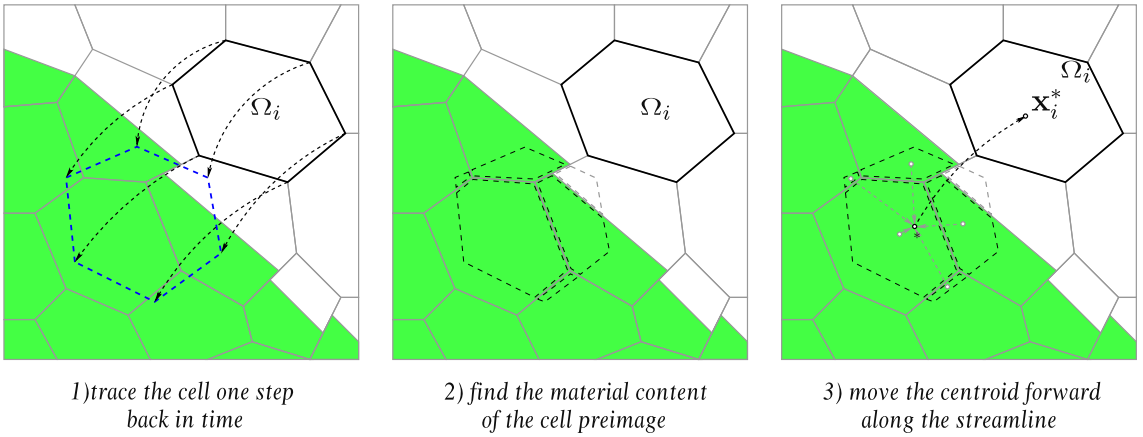

Fig. 2. The cell-wise material volumes and centroids required for the MoF interface reconstruction can be consistently updated by the means of Lagrangian remap.

the cell-wise material volume and centroids by means of *Lagrangian remap*: track the cell vertices back in time to find the Lagrangian preimage of the cell, find all the intersections of the preimage with the pure-material subcells from the previous time step, and then assign all the content of the preimage to the cell; the centroids of the material enclosed in the preimage are advected forth in time along the streamlines (Fig. 2).

In this paper we would like to show how the moment-of-fluid technique is applied to the multi-material case. Since the Lagrangian remap has no limitation on the number of material advected, there is no need to discuss the update the moment data, and we can concentrate on a stand-alone interface reconstruction problem.

The mixed-cell cell partitioning can be a real problem in the case of multiple materials. Here we demonstrate how the two-material MoF interface reconstruction algorithm can be used to perform a polygonal partitioning of a mixed cell with $M \geqslant 3$ materials. Basically, we follow the strategy of the multi-material volume-of-fluid (VoF) method and use the two-material interface reconstruction algorithm for extracting materials from the mixture one by one. There is an essential difference though: the MoF interface reconstruction does not require the user to specify the material order explicitly. *The right order is determined automatically* by trying all $M!$ possible material orders and finding the one that results in the minimal defect of the first moment.

The search of the best mixed-cell partition does not limit the choice of partitioning scheme in any way. Therefore, in order to achieve a lower defect of the first moment, one can expand the family of the trial partitions at will. For instance, instead of extracting materials from the mixture in series, one can separate them according to the "divide-and-conquer" principle: choose an arbitrary $m < M$, separate the mixture of materials $1,\ldots,m$ from $m+1,\ldots,M$, and then recursively apply this algorithm to each submixture. This procedure allows to generate $M!(M-1)!$ *B-Tree partitions* to choose from, which significantly increases the chances of finding an approximate partition that fits given moment data best.

After introducing the basic notations and formulating the problem, we review the multi-material interface reconstruction schemes used in the VoF context, and then describe and test the multi-material MoF algorithm with the two types of the mixed-cell partitionings: the *serial* and the *B-Tree partitionings* (more than three materials).

2. Problem formulation

Consider a polygon Ω that represents a mixed cell containing $M \geqslant 3$ different materials. Let ω_m be a subset of Ω that specifies the space occupied by the mth material, $m = 1,\ldots,M$. Since $\{\omega_m\}_{m=1}^{M}$ represents a *partition*, i.e. the *cell fractions* (*subcells*) occupied by different materials do not overlap and there is no void, then

$$\sum_{m=1}^{M} |\omega_m| = |\Omega|, \tag{1}$$

where $|\omega|$ denotes the volume (area) of a plane set $\omega \subset \mathbb{R}^2$.

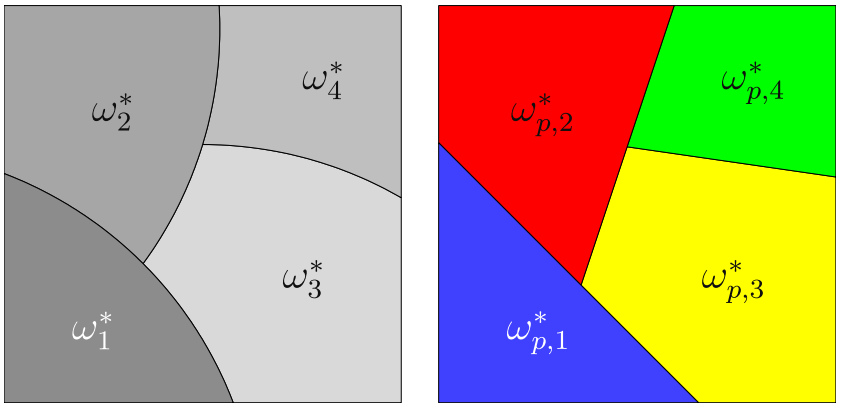

(a) true partition of a mixed cell *(b) its polygonal approximation*

Fig. 3. Example of the volume-conservative interface reconstruction.

If all the materials have polygonal shapes, the whole partition is referred to as *polygonal*; in this case we equip each subcell symbol with an extra "p" subscript: $\omega_{p,m}$.

Suppose that partition $\{\omega_m^*\}_{m=1}^M$ specifies a true distribution of materials in the mixed cell. The objective of the *volume-conservative interface reconstruction* (Fig. 3) is to *find an approximate polygonal partition* $\{\omega_{p,m}^*\}_{m=1}^M$ *of* Ω *that preserves the volumes of all materials*:

$$|\omega_{p,m}^*| = |\omega_m^*|, \quad m = 1, \ldots, M.$$

The first question one would ask is *how to measure the proximity of the partitions*? Clearly, two partition are only as close to each other as their respective material fractions. We introduce three different measures of the proximity between the true subcells and their reconstructed counterparts (Fig. 4):

- *the defect of the first moment*:

$$\Delta M_1 = ||\mathbf{M}_1(\omega_{p,m}^*) - \mathbf{M}_1(\omega_m^*)|| = |\omega_m^*|\,||\mathbf{x}_c(\omega_{p,m}^*) - \mathbf{x}_c(\omega_m^*)||,$$

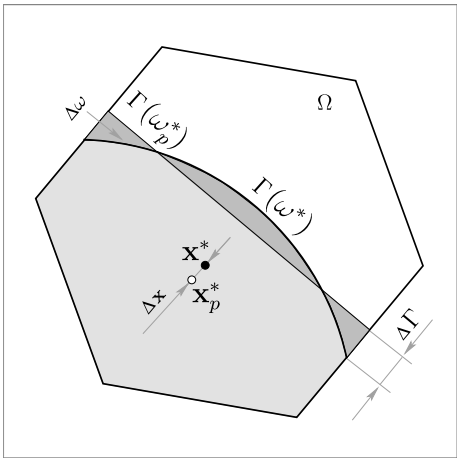

Fig. 4. The reconstruction errors illustrated. Ω is a hexagonal mixed cell, $\Gamma(\omega^*)$ and $\Gamma(\omega_p^*)$ are the true and reconstructed material interfaces, respectively. $\Delta\Gamma$ is *the maximum deviation* of the true interface $\Gamma(\omega^*)$ from the reconstructed one $\Gamma(\omega_p^*)$; $\Delta\omega$ is *the area of the symmetric difference* between the true and reconstructed subcells (in dark grey); *the defect of the first moment* ΔM_1 is proportional to the distance $\Delta\mathbf{x}$ between the true and reconstructed centroids ($\mathbf{x}^*$ and $\mathbf{x}_p^*$, respectively).

where

$$\mathbf{M}_1(\omega) = \int_\omega \mathbf{x}\,d\mathbf{x} \in \mathbb{R}^2$$

is the *first moment* of a plane set $\omega \subset \Omega$,

$$\mathbf{x}_c(\omega) = \mathbf{M}_1(\omega)/|\omega|$$

is the respective *centroid* (subject $|\omega| > 0$), and $||\mathbf{x}||$ denotes the Euclidean norm of $\mathbf{x} \in \mathbb{R}^2$;

- *the area of the symmetric difference between the true and reconstructed subcells* (*the area between the true and reconstructed interfaces*):

$$\Delta\omega = |\omega^*_{p,m} \triangle \omega^*_m| = |\omega^*_{p,m} \setminus \omega^*_m| + |\omega^*_{p,m} \setminus \omega^*_m| = 2(|\omega^*_m| - |\omega^*_m \cap \omega^*_{p,m}|);$$

- *the* (*Hausdorff*) *distance between the subcell boundaries*:

$$\Delta\Gamma = \mathrm{dist}(\partial\omega^*_{p,m}, \partial\omega^*_m) \equiv \max\left\{ \max_{\mathbf{x}\in\partial\omega^*_{p,m}} \min_{\mathbf{y}\in\partial\omega^*_m} ||\mathbf{x}-\mathbf{y}||; \max_{\mathbf{x}\in\partial\omega^*_m} \min_{\mathbf{y}\in\partial\omega^*_{p,m}} ||\mathbf{x}-\mathbf{y}|| \right\}.$$

The reasons for considering three different subcell approximation errors are the following. The defect of the 1st moment ΔM_1 is the error that is explicitly minimized in moment-based reconstruction. The symmetric-difference area $\Delta\omega$ gives the sense of the *average distance* between the true and reconstructed boundaries; we also find it convenient for direct measurements. And the $\Delta\Gamma$ error, which shows the *maximum deviation* of the reconstructed interface from the true one, is a standard choice of the reconstruction error.

The partition approximation errors can be defined as the vector-norm combinations of the respective subcell approximation errors:

- *the cumulative defect of the first moment*:

$$\Delta M_1 = \left\{ \sum_{m=1}^{M} ||\mathbf{M}_1(\omega^*_{p,m}) - \mathbf{M}_1(\omega^*_m)||^2 \right\}^{1/2},$$

- *the cumulative symmetric-difference area*:

$$\Delta\omega = \left\{ \sum_{m=1}^{M} |\,\omega^*_{p,m} \triangle \omega^*_m|^2 \right\}^{1/2},$$

- *the maximum distance between the boundaries*:

$$\Delta\Gamma = \max_{1\leqslant m\leqslant M} \mathrm{dist}(\partial\omega^*_m, \partial\omega^*_p m).$$

Among these three types of the partition approximation error, ΔM_1 is the weakest, and $\Delta\Gamma$ is the strongest one (convergence in $\Delta\Gamma$ implies convergence in $\Delta\omega$, and convergence in $\Delta\omega$ implies convergence in ΔM_1). By default the reconstruction error is measured in terms of $\Delta\Gamma$. Thus, a reconstruction is known to be kth-order accurate, if it results in $\Delta\Gamma = \mathrm{O}(h^k)$ for all sufficiently small h (the size of the cell). Since both the true and the approximate interfaces are confined within the cell, *an arbitrary partitioning is at least 1st-order accurate*. Following the common practice, we specify the order of accuracy of a reconstruction algorithm in terms of $\Delta\Gamma$. There is a simple rule to reckon the order of accuracy of a two-material interface reconstruction algorithm: if it can reproduce any linear interface exactly, the algorithm is 2nd-order accurate, otherwise it is only 1st-order accurate. In case of multiple materials one can use a similar rule: if the algorithm reconstructs any polygonal partition of a given interface topology exactly, it can reconstruct any partition of the same interface topology with twice-differentiable interfaces with 2nd-order accuracy; otherwise the algorithm is just 1st-order accurate (with respect to the partitions of the given topology).

The second question would be: *what kind of approximate mixed-cell partitions are of interest to us*? We are looking for the solution $\{\omega^*_{p,m}\}_{m=1}^{M}$ in the class of the polygonal partitions that can be obtained from Ω with a series of successive dissections (like the one shown in Fig. 3b). The main reason for this choice is that all known volume-conservative interface reconstruction methods are formulated in terms of two materials, i.e. are able to divide a mixed cell into two part (most commonly, with a linear interface). Therefore, the dissection is the simplest (and usually the only) basic operation available for constructing a multi-material partition.

3. Volume-of-fluid legacy

The volume-of-fluid (VoF) methods perform the volume-conservative interface reconstruction based on the cell-wise material volume data only. As we have mentioned in the introduction, all VoF interface reconstruction algorithms rely on the material volume data from the direct neighbors of the mixed cell. Therefore in the course of this section we always assume that Ω is surrounded by other cells that provide the data for the evaluation of the interface normals.

3.1. The partitioning scheme choices

We were able to identify four different partitioning schemes based of the two-material interface reconstruction (Fig. 5). Since there is no established name convention for the multi-material interface reconstruction schemes, we took the liberty to come up with our own.

Partitioning scheme 1 (Independent Dissections (ID), mentioned in [5]). *In a completely independent manner calculate M linear interfaces inside Ω, such that the mth interface, $m = 1, \ldots, M$, separates the mth material from the rest.*

The mth material occupies the space $\omega^*_{p,m}$ behind the mth interface, $m = 1, \ldots, M$.

Since the reconstruction preserves the material volumes, the cell fractions $\{\omega^*_{p,m}\}_{m=1}^{M}$ obtained with the Independent Dissections inevitably overlap, leaving the room for a void. The resulting material distribution

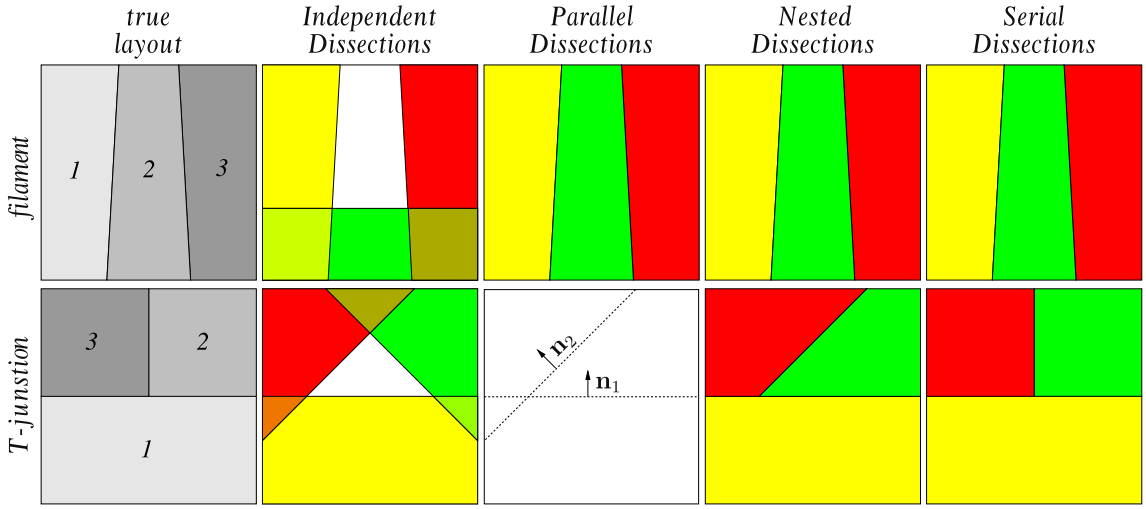

Fig. 5. Two different material layouts on the left: a filament and a T-junction; and their reconstructions obtained with various partitioning schemes. The true interfaces have no curvature and extend linearly to the direct neighbors. The material order used for reconstruction is specified on the true layouts. Independent Dissections (second column) always result is material overlaps and form a void. There is no difference between the Parallel, Nested, and Serial Dissections in reconstructing a layered material structure (top row), but their reconstructions of a T-junction (bottom row) are quite different: the Parallel Dissections fail, because the interface bounding material 1, and the interface bounding the mixture of materials 1 and 2 do intersect, the Nested Dissections deliver only 1st-order accurate result, while the Serial Dissections are 2nd-order accurate (reconstruct polygonal partitioning exactly).

in a mixed cell is completely unphysical ($\{\omega^*_{p,m}\}_{m=1}^{M}$ is not a valid partition of Ω), but still may be considered acceptable by those who perform the reconstruction in hydrodynamic simulations just to decrease the diffusion of the interfaces. With $M \geqslant 3$ at least one subcell in any polygonal partition has a non-linear interface (it could be several separate linear segments, one or several separated polylines); one can not reproduce it exactly with a single linear segment. Therefore, this algorithm is always 1st-order accurate. On the positive side, all M interfaces can be calculated in parallel.

Partitioning scheme 2 (Parallel Dissections (PD), commonly referred to as the "*onion-skin*" *model* [23,5]). *Given a particular material order, in a completely independent manner calculate* $M-1$ *linear interfaces inside* Ω, *such that the mth interface,* $m = 1, \ldots, M-1$, *separates the mixture of the first m materials from the rest.*

If the mth interface is located behind the $(m+1)$*th one for all* $m = 1, \ldots, M-2$, *then the partitioning can be completed successfully, otherwise the partitioning fails. In the former case the resulting interfaces do not intersect (are "parallel"), and therefore the materials can be placed as follows:*

(1) *the 1st material occupies the space* $\omega^*_{p,1}$ *behind the 1st interface,*
(2) *the 2nd material occupies the space* $\omega^*_{p,2}$ *between the 1st and the 2nd interfaces,*
⋮
(m) *the mth material occupies the space* $\omega^*_{p,m}$ *between the* $(m-1)$*th and the mth interfaces,*
⋮
(M) *at last, the Mth material occupies the space* $\omega^*_{p,M}$ *in front of the* $(M-1)$*th interface.*

All the PD interfaces can be calculated in parallel, but a posteriori one has to check whether they define a valid partition, i.e. whether the *mth* interface is actually located behind the $(m+1)$*th* interface, $m = 1, \ldots, M-2$.

The Parallel Dissections can successfully resolve the layered material structure, but it is impossible to guarantee the success of the Parallel Dissections in a more general case.

Under the assumptions that:

(1) the true partition is C^2-*parallel* (i.e. the interfaces do not intersect and are C^2-differentiable),
(2) the right material order is given,
(3) the (two-material) interface reconstruction algorithm used is 2nd-order accurate.

The Parallel Dissections are 2nd-order accurate; this follows from the obvious fact that any polygonal parallel partition under the conditions (2) and (3) will be reconstructed by the Parallel Dissections exactly. Note that, for any C^2-parallel partition there exist two (mutually reversed) material orders that yield a 2nd-order accurate result with the Parallel Dissections.

Partitioning scheme 3 (Nested Dissections (ND) [11]). *Given a particular material order, in a completely independent manner calculate the normals of all* $M-1$ *Parallel Dissections interfaces (the actual locations of the PD interfaces are irrelevant).*

The materials are separated from the bulk one by one as follows:

(1) *The 1st material* $\omega^*_{p,1}$ *is separated from the cell* Ω *with the linear interface that has the same normal as the 1st PD interface. The remaining part of the cell*
$\omega_{p,2+} \equiv \Omega \setminus \omega^*_{p,1}$
is further divided between the materials 2 through M.
(2) *The 2nd material* $\omega^*_{p,2}$ *is separated from* $\omega_{p,2+}$ *with the linear interface that has the same normal as the 2nd PD interface. The remaining part of* $\omega_{p,2+}$
$\omega_{p,3+} \equiv \omega_{p,2+} \setminus \omega^*_{p,2}$
is further divided between the materials 3 through M.⋮
(m) *The mth material* $\omega^*_{p,m}$ *is separated from* $\omega_{p,m+}$ *with the linear interface that has the same normal as the mth PD interface. The remaining part of* $\omega_{p,m+}$

$\omega_{p,(m+1)+} \equiv \omega_{p,m+} \setminus \omega^*_{p,m}$

is further divided between the materials $m+1$ through M.⋮

(M) *Finally, the remaining space $\omega^*_{p,M}$ is intended for the Mth material.*

The construction of the interfaces in this case can not be parallelized completely: although the evaluation of the normals can be carried out in parallel, their actual locations can be identified only in series.

The Nested Dissections scheme can be viewed as a robust modification of the Parallel Dissections. Indeed,

- it always results in a valid partition,
- the ND and PD interface normals are always identical, and
- the ND and PD partitions are also identical, unless the Parallel Dissections fail.

Contrary to the Parallel Dissections, the Nested Dissections scheme does not require the materials to be layered to get a valid partition. The result of the ND partitioning can be classified as a *polygonal serial partition*. A mixed-cell partition is called C^2-*serial*, if all the materials can be separated from the bulk one by one with C^2-differentiable interfaces. If the separating interfaces are linear, then the C^2-serial partition is polygonal. Parallel partition, introduced above, is a serial partition with non-intersecting interfaces.

One may think that it is possible to get a 2nd-order accurate ND reconstruction of any C^2-serial partition. Unfortunately, it is not true: the Nested Dissections are 2nd-order accurate only under the same conditions as the Parallel Dissections are. The ND approximation to the C^2-serial partition with intersecting interfaces is only 1st-order accurate. This statement can be explained with a simple *T-junction* example (Fig. 5, bottom row) The true interface bounding the group of the first two materials (the right order is assumed) is non-smooth, and therefore its PD approximation is only 1st-order accurate, which automatically prohibits the accuracy order of the ND reconstruction to be higher than 1.

We could not find any description of the Nested Dissections in literature; our knowledge of this partitioning scheme comes from Garimella [11].

Partitioning scheme 4 (Serial Dissections (SD)). *Given a particular material order, separate materials from the bulk one by one as follows:*

(1) *Construct the linear interface that separates the 1st material $\omega^*_{p,1}$ from the cell Ω. The remaining part of the cell*

$\omega_{p,2+} \equiv \Omega \setminus \omega^*_{p,1}$

is further divided between the materials 2 through M.

(2) *Construct the linear interface that separates the 2nd material from $\omega_{p,2+}$. The remaining part of $\omega_{p,2+}$*

$\omega_{p,3+} \equiv \Omega \setminus \omega^*_{p,2}$

is further divided between the materials 3 through M.⋮

(m) *Construct the linear interface that separates the mth material from $\omega_{p,m+}$. The remaining part of $\omega_{p,m+}$*

$\omega_{p,(m+1)+} \equiv \Omega \setminus \omega^*_{p,m}$

is further divided between the materials $m+1$ through M.⋮

(M) *Finally, the remaining space $\omega^*_{p,M}$ is intended for the Mth material.*

The construction of the individual interfaces by this partitioning scheme is completely serial. When evaluating an interface normal, the Serial Dissections, unlike the Nested Dissections, take into account the fact that some fraction of the cell interior has already been occupied by the higher-priority materials; this gives a chance to calculate the interface normal with higher accuracy.

In order to get a 2nd-order accurate SD reconstruction of a C^2-serial partition, it is absolutely essential to separate the materials in adjacent multi-material cells synchronously. This requirement is explained by the need to use the material volume data from the direct neighbors of the mixed cell for the evaluation of the interface normal; in order to construct a 2nd-order accurate interface approximation, it is important to eliminated

from consideration the space already occupied by all the preceding materials not only inside the mixed cell, but also inside its direct neighbors. Therefore, a 2nd-order accurate SD reconstruction is feasible only for an isolated cluster of adjacent multi-material cells that share a common material order.

When it comes to reconstructing a layered material structure, the Serial Dissections are more tolerant to the material order choice than the Parallel Dissections: for any C^2-serial partition there exist 2^{M-1} different material orders that yield a 2nd-order accurate result with the Serial Dissections.

The requirement to construct the interfaces in adjacent mixed cells in sync makes the Serial Dissections implementation in the VoF context cumbersome. We could not find any description of the Serial Dissections in literature, but there is an evidence that this partitioning scheme is in use in LLNL [1].

After reviewing the partitioning schemes used with VoF, one may conclude that the multi-material interfaces reconstructed from the volume data can be 2nd-order accurate only for the layered and, conditionally, for the serial material structure (all the interface between adjacent materials must be twice-differentiable).

3.2. The material ordering choices

All the multi-material partitioning schemes presented (save the Independent Dissections, which is not a valid partitioning scheme per se) rely on the user-defined material order. Since the right choice of the material order is crucial for the accurate reconstruction, a robust strategy for prioritizing the materials is of high importance.

A convenient way to avoid this problem is to delegate the responsibility to determine the material order to the end user. Nobody expects the user to intervene each time a multi-material interface reconstruction routine is called; but the user can be helpful defining a fixed material order. For many problems in impact and penetration, where the materials are known to keep the initial layer structure, the fixed order works well, but there are simple interface configurations (like the Δ-junction shown in Fig. 15c or the "parquet" configuration from Fig. 20), for which no fixed material order will work.

We are aware of three *dynamic* priority systems that can be used in static interface reconstruction[1]:

- Bailey [2] defines the material priority as the number of the surrounding cells containing the material. This tactics determines the right sequence of the Serial Dissections (not the Parallel Dissections!) for a single filament co-aligned with the grid lines (Fig. 6a), but not for a diagonal filament (Fig. 6b).
- Mosso and Clancy [15] developed the system based on the approximate material centroids. They consider a 3×3 cell block that includes a mixed cell with all its direct neighbors and calculate the approximate centroids $\{\tilde{\mathbf{x}}_m\}_{m=1}^{M}$ of the materials inside the block from the material volume data; for this purpose the cell-wise material centroids are approximated by the cell centers:

$$\tilde{\mathbf{x}}_m = \left\{ \sum_{i=1}^{9} |\omega_{m,i}| \right\}^{-1} \sum_{i=1}^{9} \mathbf{x}_c(\Omega_i) |\omega_{m,i}|, \quad m = 1, \ldots, M,$$

  here index i is used to specify a cell withing the 3×3 cluster. After all the centroids are evaluated, the materials are arranged in the ascending order of their centroid distances from the *origin*; the origin is located at the north–west corner of the 3×3 block, if the set of the centroids has a dominantly negative slope (Fig. 7a), and at the south–west corner otherwise.

  The Mosso–Clancy system correctly determines the material order for a single filament (Fig. 7a), but may give a wrong answer for a T-junction or for the layered materials of number 4 and more.Fig. 7b shows an example of the T-junction, for which the Mosso–Clancy system assigns the priorities incorrectly: the dark material on the right, although has to be separated the first, is assigned the lowest priority. We would like to point out that there is some ambiguity in the origin location for this particular configuration. The rule for estimating the slope of the centroid set is not deterministic in this case, and, depending on the choice of the

[1] We discuss here neither the CTH-code priority systems by McGlaun (mentioned in [5]) and by Bell and Hertel [4], nor the priority system for simulations with background material by Benson [6,7]: the systems used in the CTH code can not be used in static interface reconstruction, since their heuristics depend on the direction of the fluid flow, and the background-material priority system is not entirely dynamic, since the background material is assigned the fixed priority.

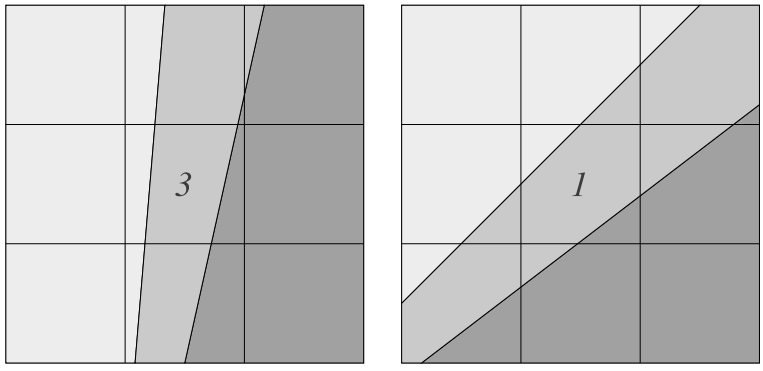

Fig. 6. (a) The Bailey's system correctly assigns the lowest priority to the filament material, if the filament is co-aligned with the grid lines; (b) it erroneously assigns the highest priority to filament material, if the filament is the dominantly diagonal. The numerical labels above specify the sequence number (reversed priority) of the material.

centroid to start with, may place the origin at either the north–west or south–west corner. Neither choice of the origin location helps the Mosso–Clancy system determine the right material order for this T-junction. Fig. 7c shows an example of the four-material parallel partition, for which the approximate centroids of two materials coincide. The Mosso–Clancy system does not have a recipe for this case. To make the situation even worse, one can break the symmetry of this configuration by rotating the interface between the filaments around the cell center. If the interface rotates counterclockwise, the approximate centroid of the right filament moves up, and the approximate centroid of the left filament moves down. For all sufficiently small rotation angles the origin location stays at the north–west corner, and, according to Mosso and Clancy, the right-filament material has higher priority over the left-filament material, which is not correct.

- Another priority system that relies on the material centroids was developed by Benson [6]. He does not derive the centroid locations from the volume data, like Mosso and Clancy do, but considers the material centroids to be independent parameters of the system and keeps track of them explicitly; strictly speaking,

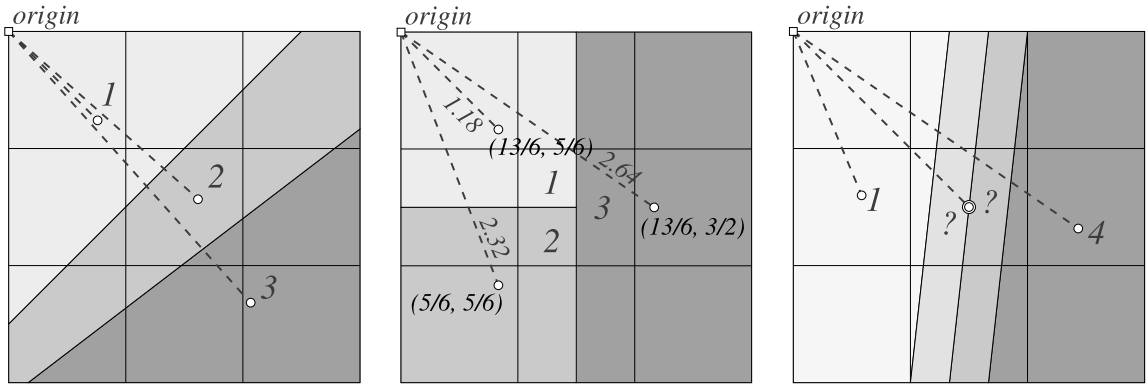

Fig. 7. (a) The Mosso–Clancy system assigns higher priority to the material, whose approximate centroid is located closer to the *origin* (the north–west or south–west corner of the 3×3 cluster). (b) An example of the T-junction, for which the Mosso–Clancy priority system assigns the lowest priority to the material that has to be separated first. (c) An example of the layered material structure with coinciding approximate centroids, for which the Mosso–Clancy system can not assign the priorities correctly.

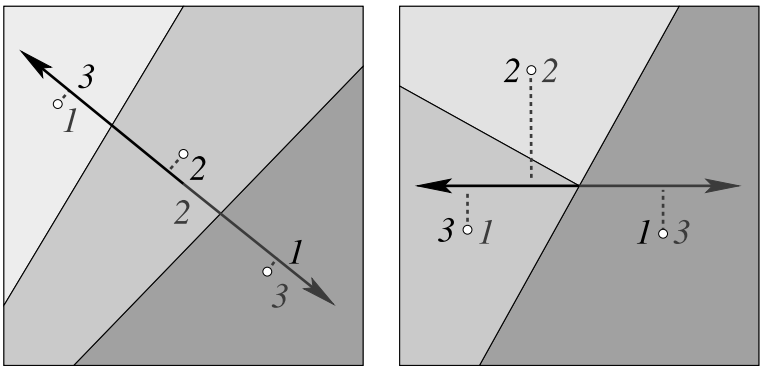

Fig. 8. The Benson's system assigns the priorities according to the order of the material centroid projections on the line resulting from the least square fit to the set of the centroids. There are two different material orders to choose from: the forward (grey) and reverse (black). When the materials in the true partition are layered, like on picture (a), it does not pose a problem: both orders are equivalent for the partitioning purposes and result in the same approximate partition. Otherwise, if the true interfaces form a junction, like on picture (b), these two orders are not equivalent, and at least one of them is wrong.

this feature prohibits the Benson's priority system from being classified as volume-based (VoF).The material order is given by the order of the centroid projections on the line determined by the least square fit to the set of the centroids. This strategy successfully recovers the order of the layered materials even when their number is high.

Note that the line to project the centroids on does not have a fixed positive direction. Depending on the choice of the positive direction (which is completely arbitrary), one may get either the forward or the reverse material order (see Fig. 8). For the layered material structure (Fig. 8a) these two orders are equivalent: the Parallel Dissections will result in the same partition anyway. But if the true interfaces form a junction (Fig. 8b), at least one of the orders is wrong. Unfortunately, there is no way to distinguish between the right and the wrong orders in this case.

Therefore, it is true to say that the material order can be confidently determined from the cell-wise material volume data only for the layered material structure.

4. Moment-of-fluid perspective

In addition to material volumes $\{|\omega_m^*|\}_{m=1}^M$, the moment-based interface reconstruction requires the material centroids $\{\mathbf{x}_m^*\}_{m=1}^M$, where $\mathbf{x}_m^* \equiv \mathbf{x}_c(\omega_m^*)$, $m = 1, \ldots, M$. One can see that in 2D material the cell-wise material centroids and volumes, provide 3 times more information than the volumes alone. This extra information can definitely be used to improve the quality of the interface reconstruction over the traditional volume-base methods.

4.1. The partitioning scheme choices

Each of the multi-material partitioning schemes described in the previous section can be transparently combined with the two-material MoF algorithm. There is an essential difference though. The MoF reconstruction does not depend on the data from the adjacent cells. This fact makes the Serial Dissections, so cumbersome and restrictive with VoF, the most suitable partitioning scheme for MoF: there is no need to synchronize the construction the interfaces in adjacent multi-material mixed cells to get a 2nd-order accurate result.

With the right material order, the SD reconstruction of a C^2-serial partition is 2nd-order accurate; the SD reconstruction of a polygonal serial partition is exact.

4.2. Automatic material ordering

The major advantage of the MoF approach over the VoF one is that it can derive the right material order automatically. The governing principle of the moment-based interface reconstruction is *finding the volume-preserving mixed-cell partition that minimizes the defect of the first moment*. In the two-material case this principle is used to determine the direction of the interface normal; in the multi-material case, it can be used to find the right material order for the Serial Dissections. Strictly speaking, the right material order is determined indirectly by performing the SD partitioning for each possible material order and choosing the one that results in the minimal defect of the first moment (see Fig. 9).

Algorithm 1 (Multi-material MoF). *Given a partitioning scheme, generate all possible trial partitions. For every trial partition* $\{\omega_{p,m}\}_{m=1}^{M}$ *evaluate the cumulative defect of the first moment*

$$\Delta\mathbf{M}_1\left(\{\omega_{p,m}\}_{m=1}^{M}\right) = \left\{\sum_{m=1}^{M} ||\mathbf{M}_1(\omega_{p,m}) - \mathbf{M}_1(\omega_m^*)||^2\right\}^{1/2} = \left\{\sum_{m=1}^{M} |\omega_m^*|\,||\mathbf{x}_c(\omega_{p,m}) - \mathbf{x}_c(\omega_m^*)||^2\right\}^{1/2}.$$

Choose the partition $\{\omega_{p,m}^*\}_{m=1}^{M}$ *that results in the minimal defect.*

Whenever used in combination with the Serial Dissections partitioning scheme, the multi-material MoF algorithm will be referred to as MoF–SD. Such an algorithm has combinatorial complexity in the number of materials: to get the answer, one has to try all $M!$ material orders. On the other hand, it is reasonable to expect only a limited number of the mixed cells in the whole computational grid to contain more than 2 materials. Therefore, for a moderate M, the computational overhead, associated with the optimal order search, is not likely to be significant. Also, the various material orders can be effectively tried in parallel.

The multi-material MoF algorithms tries to place the materials as close to their true locations as possible. If the true partition is polygonal serial, then there exists a material order, for which the Serial Dissections result

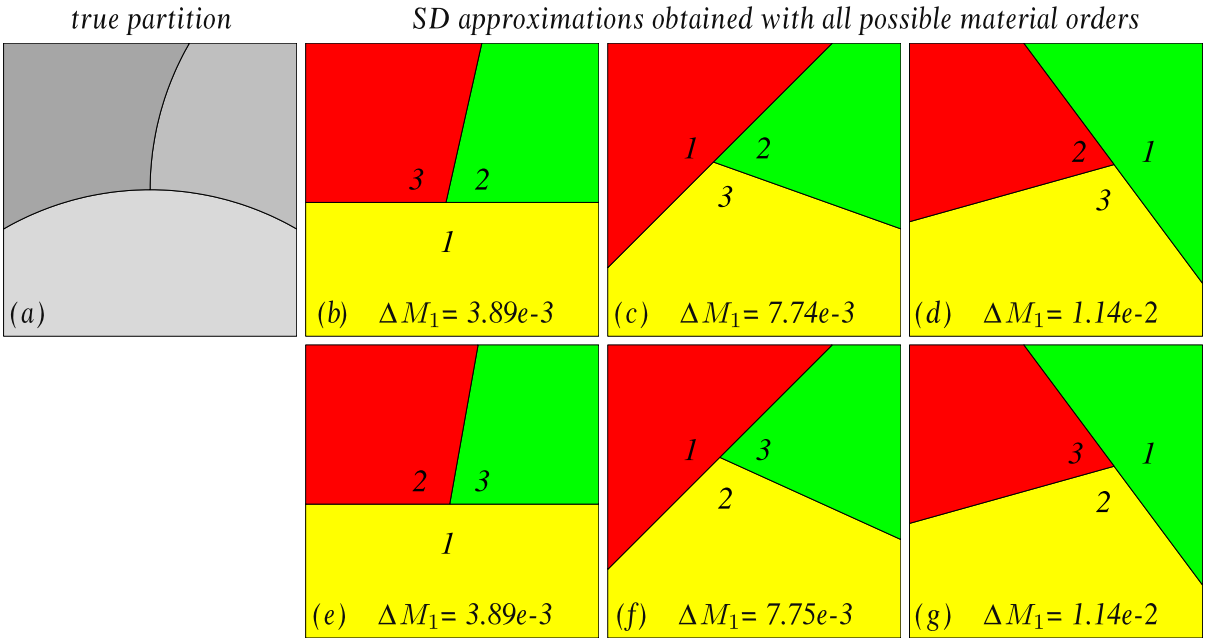

Fig. 9. As an illustration of the multi-material MoF strategy, we present here a C^2-*serial* partition (a) and its SD approximations obtained with all possible orders (b–g); at the bottom of each approximate partition we specify the respective (cumulative) defect of the first moment. Note that, as long as the curvature of true interfaces is moderate (in our case the curvature radius $R = h$), the order of the last two materials is not important. The approximate partition obtained with the right material orders (b and e) result in the lowest defect.

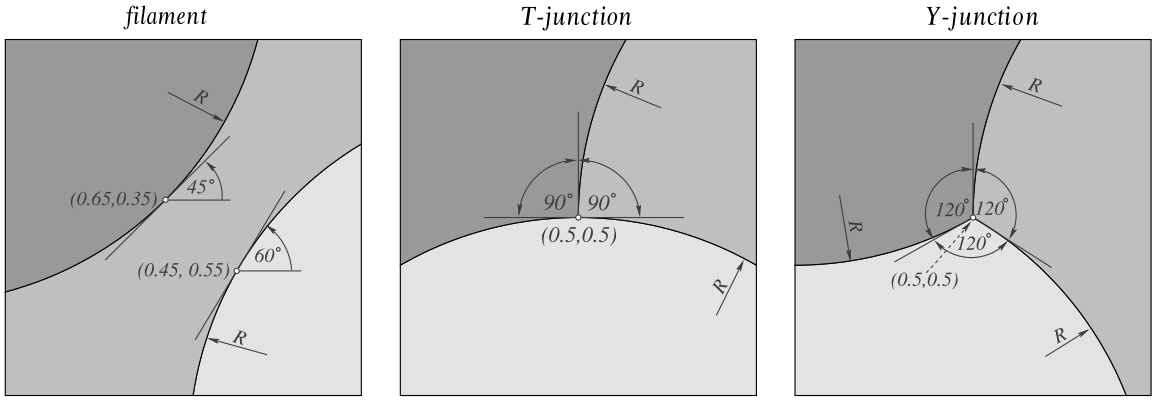

Fig. 10. Three types of the three-material cell mixed-cell layouts. The filament and the T-junction are examples of C^2-serial partitions, but the Y-junction is not. The coordinates of the points are given in h (size of the cell) units. All the interfaces have the same curvature $1/R$.

in the exact reconstruction. The exact reconstruction has zero defect of the first moment. And, since *the polygonal serial partition is uniquely identified by the set of the material centroids* (*the first moments*), any other trial serial partition should have a non-zero defect, i.e. can not be a minimizer. The last observation, along with the fact that the first-moment defect continuously changes with the shape of the subcells, suggests that the MoF–SD algorithm should guess the material order correctly not only for a polygonal serial partition, but also for any C^2-serial partition with the sufficiently low interface curvature.

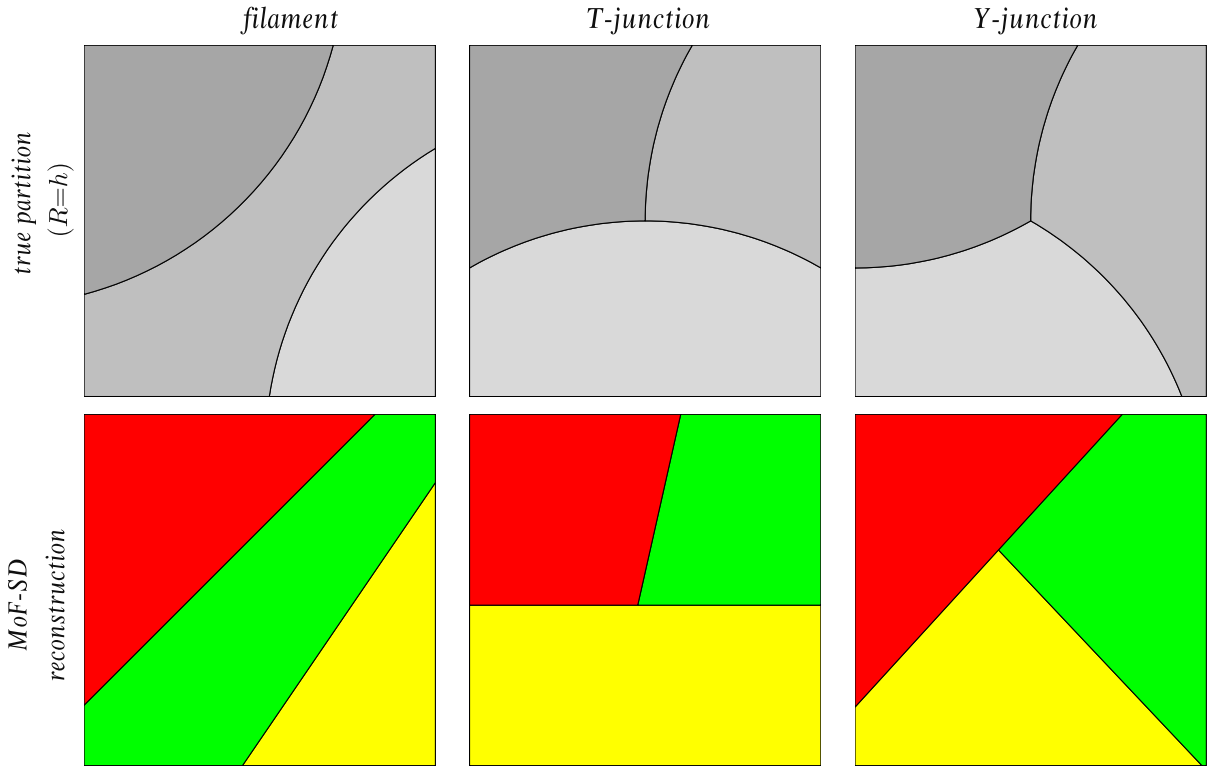

Fig. 11. The test partitions (top row, the radius of the interface curvature $R = h$) and their MoF reconstructions obtained with the Serial Dissections (bottom row). The MoF algorithm tries to place the materials as close as possible to their true locations, even when the structure of the true partition is beyond the scope of the partitioning scheme (the Y-junction).

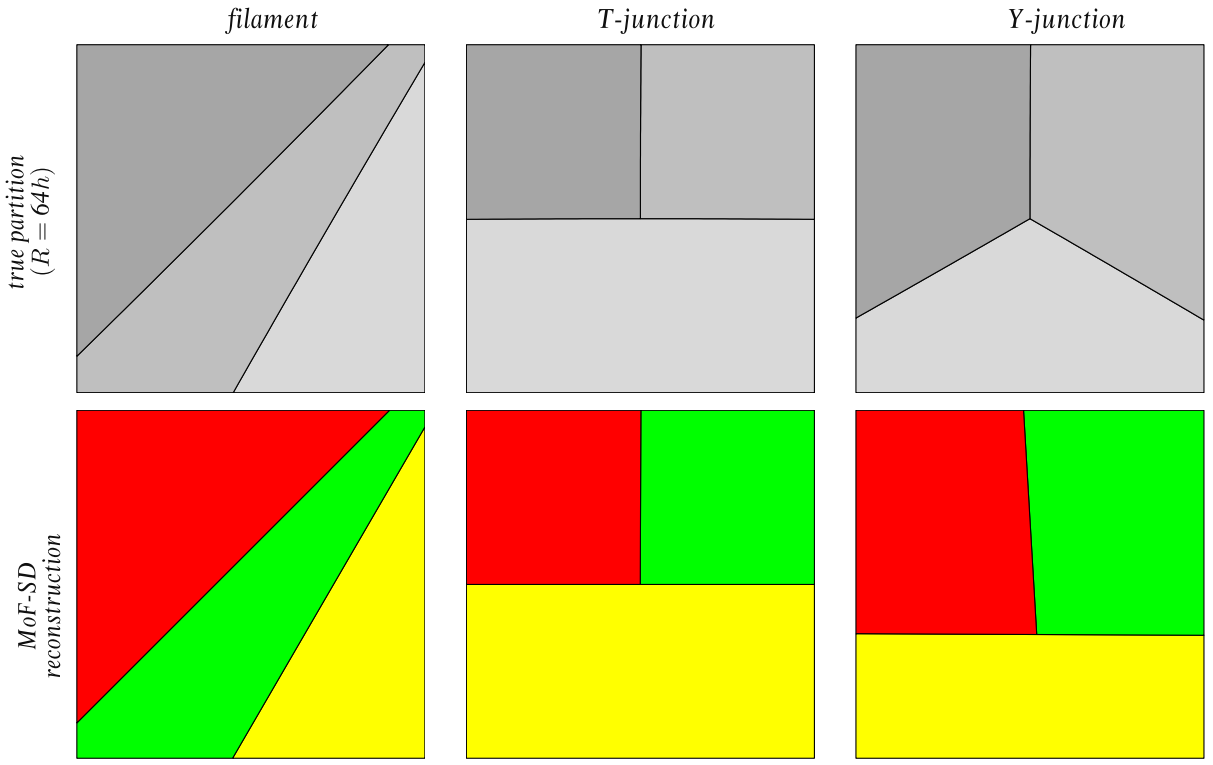

Fig. 12. The test partitions (top row, the radius of the interface curvature $R = 64h$) and their MoF–SD reconstructions (bottom row). As the interface curvature vanishes, the MoF–SD reconstructions of the C^2-serial layouts (the filament and the T-junction) converges to their respective true partitions.

We claim that the MoF–SD algorithm results in the 2nd-order accurate approximation to any C^2-serial partition.

4.2.1. Numerical tests

To support our claim, we tested three different mixed-cell layouts (see Fig. 10):

- a filament (no junction),
- a T-junction and
- a Y-junction.

The first two configurations are C^2-serial partitions, the third one is not. The examples of the moment-based reconstructions of these interface configurations for $R = h$ and $R = 64h$ are presented in Figs. 11 and 12, respectively.

Each of the three setups above is described by two parameters: the size of the cell h and the curvature $1/R$ of the interfaces, which allow a unique non-dimensional combination h/R. The interface reconstruction errors $\Delta\mathbf{M}_1$, $\Delta\omega$, and $\Delta\Gamma$, introduced in Section 2, should also be the functions of these two parameters. It is clear that if the h/R ratio is fixed, then the interface reconstruction errors scale according to their respective dimensions:

$$\Delta M_1 = \mathrm{O}(h^3),$$
$$\Delta\omega = \mathrm{O}(h^2),$$
$$\Delta\Gamma = \mathrm{O}(h),$$

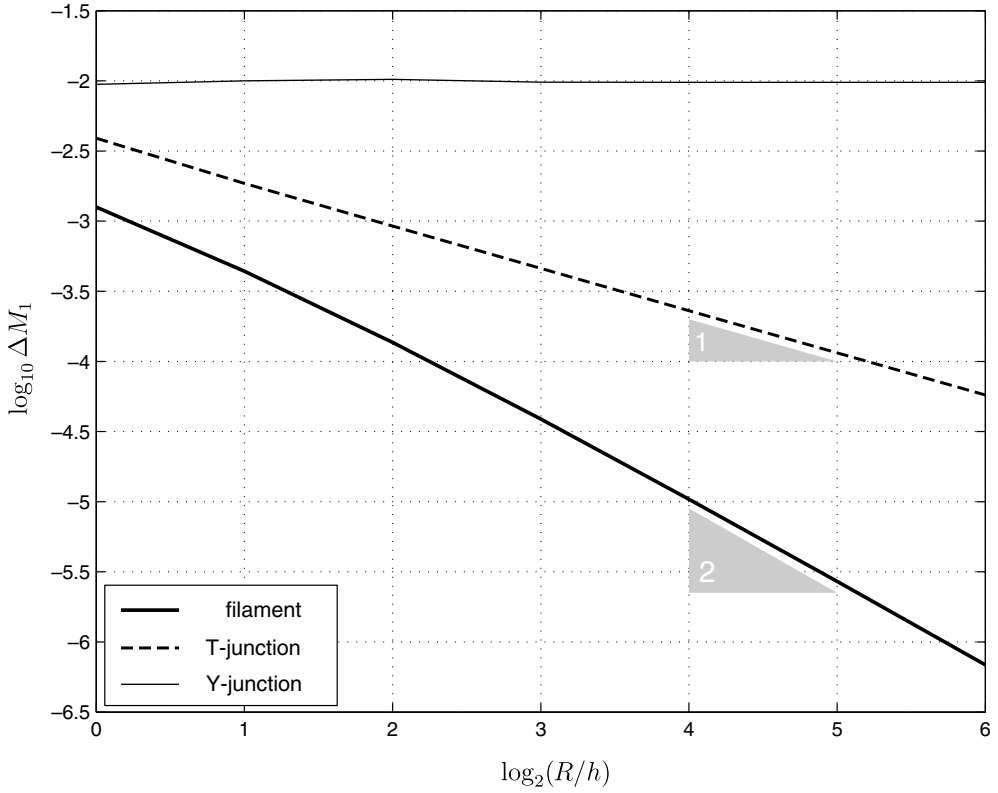

$\log_2(R/h)$	ΔM_1 error		
	filament	T-junction	Y-junction
0	1.26e-3	3.89e-3	9.44e-3
1	4.39e-4	1.86e-3	1.00e-2
2	1.37e-4	9.22e-4	1.02e-2
3	3.88e-5	4.60e-4	9.80e-3
4	1.04e-5	2.30e-4	9.77e-3
5	2.70e-6	1.15e-4	9.76e-3
6	6.87e-7	5.75e-5	9.76e-3

Fig. 13. The cumulative defect of the first moment ΔM_1 as a function of the interface curvature $1/R$ (the size of the mixed cell is fixed $h = 1$).

the expressions above may include the interface curvature only as a part of a non-dimensional constant:

$$\begin{aligned} \Delta M_1 &= \mathrm{O}((h/R)^{\alpha_1} h^3), \\ \Delta\omega &= \mathrm{O}((h/R)^{\alpha_2} h^2), \\ \Delta\Gamma &= \mathrm{O}((h/R)^{\alpha_3} h), \end{aligned} \tag{2}$$

where the exponents $\alpha_1, \alpha_2, \alpha_3$ depend only on the type of the junction and can be identified through the direct error measurements.

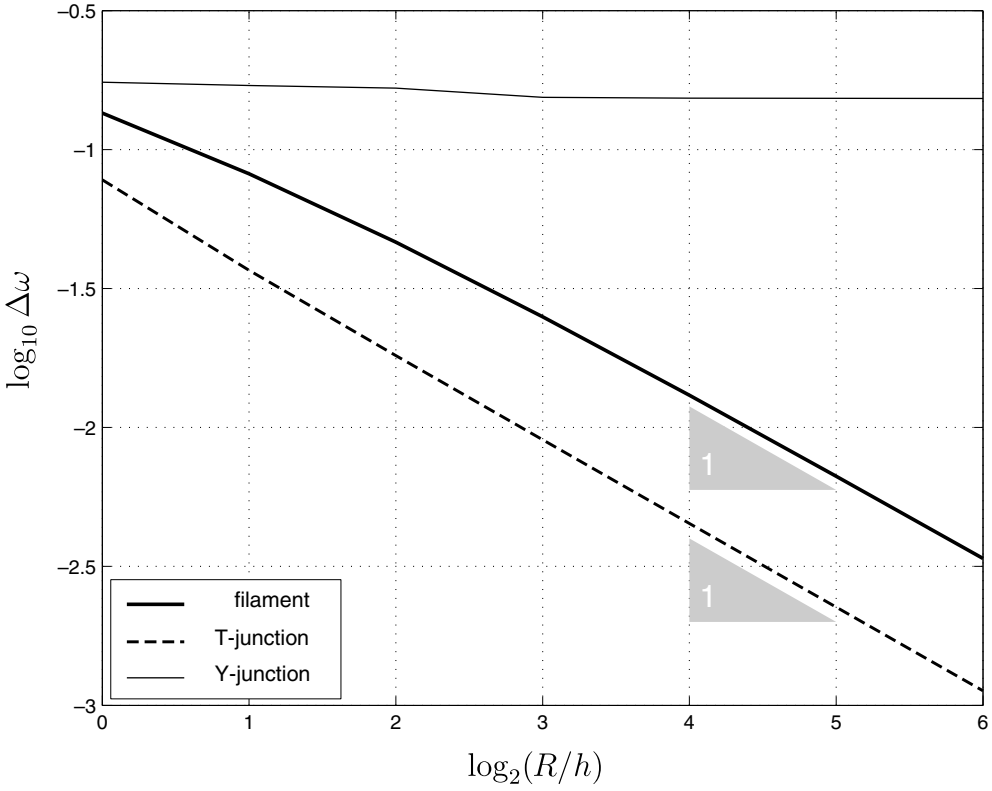

$\log_2(R/h)$	$\Delta\omega$ error		
	filament	T-junction	Y-junction
0	1.35e-1	7.78e-2	1.75e-1
1	8.19e-2	3.68e-2	1.70e-1
2	4.64e-2	1.81e-2	1.66e-1
3	2.50e-2	9.04e-3	1.54e-1
4	1.31e-2	4.51e-3	1.53e-1
5	6.67e-3	2.26e-3	1.53e-1
6	3.36e-3	1.13e-3	1.53e-1

Fig. 14. The cumulative symmetric-difference area $\Delta\omega$ as a function of the interface curvature $1/R$ (the size of the mixed cell is fixed$h = 1$).

To find the exponents α_1 and α_2 for a particular type of the interface junction, we fixed the size of the mixed cell $h = 1$ and measured the dependence of the ΔM_1 and $\Delta\omega$ errors on the interface curvature; the results are presented in Figs. 13 and 14. By evaluating the slopes of the error graphs, one may conclude that for the filament $\alpha_1 = 2, \alpha_2 = 1$, for the T-junction $\alpha_1 = \alpha_2 = 1$, and for the Y-junction $\alpha_1 = \alpha_2 = 0$.

Since the direct measurement of the maximum distance $\Delta\Gamma$ between the true and the reconstructed interfaces is somewhat tricky, we decided to use geometrical considerations to find α_3. Let us take a look at the *average deviation* $\overline{\Delta\Gamma}$ *of the reconstructed interface from the true one*, which we define as

$$\overline{\Delta\Gamma} = \Delta\omega/|\Gamma|,$$

where $|\Gamma| = O(h)$ is the total length of the true interfaces inside the mixed cell. Since the true interfaces in our experiments are piecewise-circular and the reconstructed ones are polygonal, $\overline{\Delta\Gamma}$ *and* $\Delta\Gamma$ *are equivalent*, i.e. for each particular type of the interface junction there exist constants $0 < c_1 \leqslant c_2$ independent of both h and R, such that

$$c_1\overline{\Delta\Gamma} \leqslant \Delta\Gamma \leqslant c_2\overline{\Delta\Gamma}.$$

Therefore,

$$\Delta\Gamma = O(\overline{\Delta\Gamma}) = O(\Delta\omega/|\Gamma|) = O(\Delta\omega/h),$$

which along with (2) results in $\alpha_3 = \alpha_2$.

Table 1 summarizes the asymptotic behavior of the interface reconstruction errors. The MoF–SD reconstruction is 2nd-order accurate, as long as the true partition is C^2-serial (the filament or the T-junction); for the Y-junction it is only 1st-order accurate.

4.3. Automatic material aggregation

The search of the best approximate mixed-cell partition, performed by the multi-material MoF algorithm, does not limit the choice of partitioning scheme in any way. Therefore, in order to achieve a lower defect of the first moment, one may expand the family of trial partitions at will. When a mixed cell contains four or more materials, the Serial Dissections partitioning scheme yields a simple but powerful generalization: instead of separating materials from the mixed cell one by one, one may recursively separate the *groups of materials*.

Partitioning scheme 5 (B-Tree Dissections (BTD)). *Given a particular material order, pick an arbitrary m between 1 and* $M - 1$ *to construct the linear interface that separates the first m materials from the rest, and then recursively subdivide these two groups until all the materials are completely separated. The input moments for separating a group of materials are given by the sum of the respective moments of all the constitutive materials.*

Table 1
The asymptotic ($h \ll R$) behavior of the interface reconstruction errors

Error	Filament	T-junction	Y-junction
ΔM_1	$O(h^5/R^2)$	$O(h^4/R)$	$O(h^3)$
$\Delta\omega$	$O(h^3/R)$	$O(h^3/R)$	$O(h^2)$
$\Delta\Gamma$	$O(h^2/R)$	$O(h^2/R)$	$O(h)$

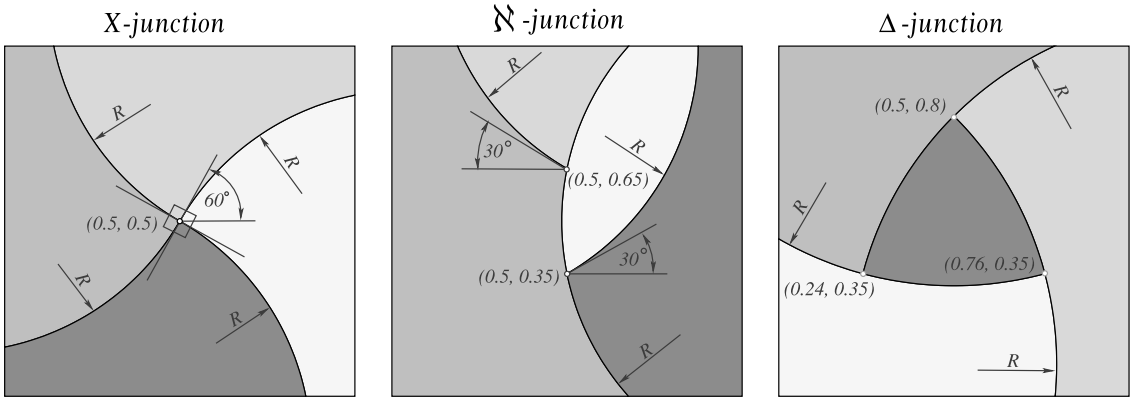

Fig. 15. Three types of the four-material mixed-cell layouts. The coordinates of the points are given in h (size of the cell) units. All the interfaces have the same curvature $1/R$.

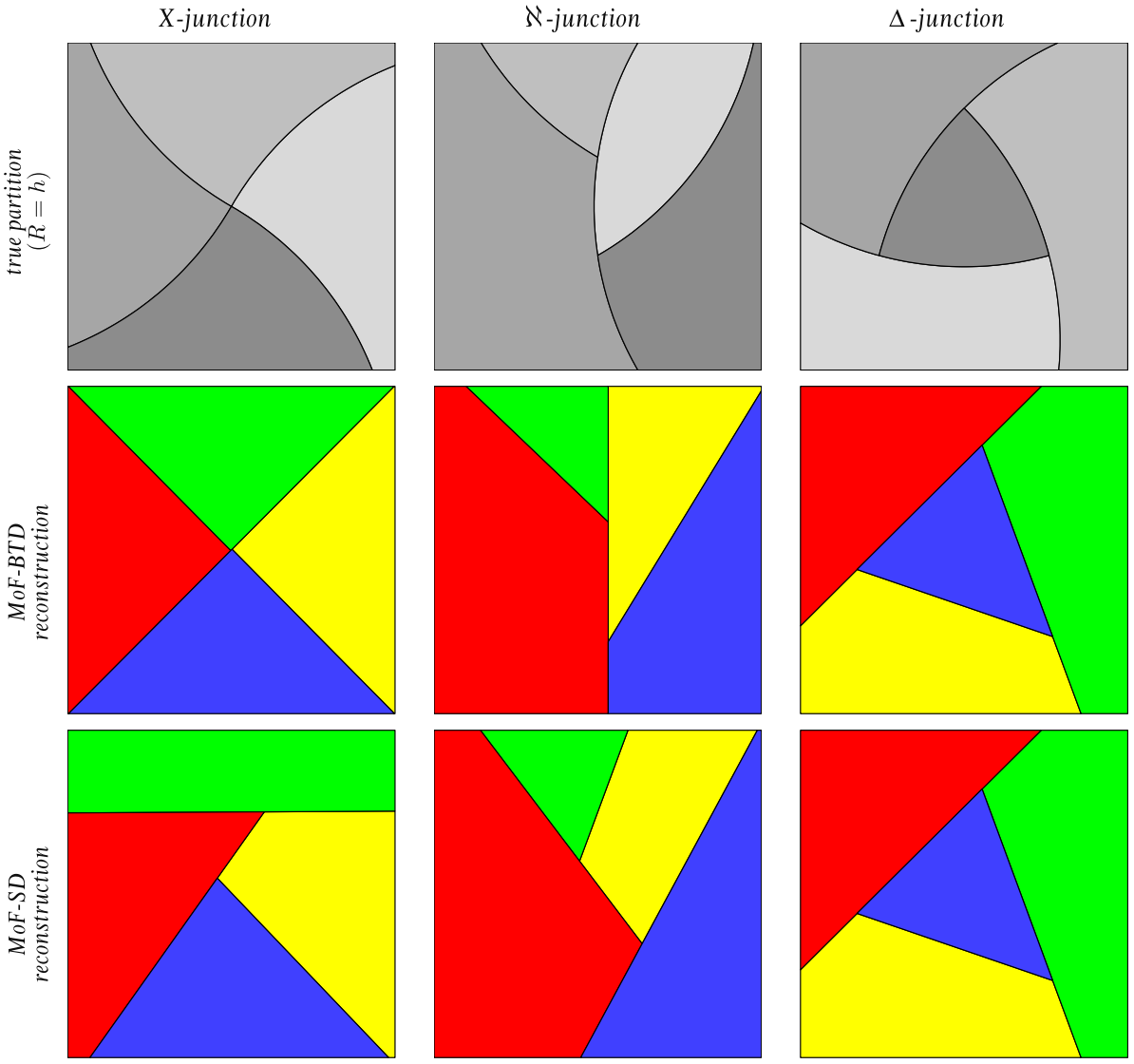

Fig. 16. The test partitions (top row, the radius of the interface curvature $R = h$) and their MoF reconstructions obtained with the B-Tree Dissections (middle row) and the Serial Dissections (bottom row). The MoF algorithm tries to put the materials as close to their true locations as possible, even when the structure of the true partition is beyond the scope of the partitioning scheme (the Δ-junction layout is beyond the scope of the B-Tree Dissections, all three layouts are beyond the scope of the Serial Dissections).

This "divide-and-conquer" partitioning algorithm generates $(M-1)!$ different partitions for a given material order, which comes to the total of $M!(M-1)!$ trial B-Tree partitions, compared to the total of $M!$ trial serial partitions. With a greater number of trial partitions available, one can explore a more diverse family of the interface layouts, and, therefore, has higher chances to attain a lower defect of the first moment.

The price one have to pay for these virtues is the higher complexity (additional factor of $M-1!$ compared to the MoF–SD) of the multi-material MoF algorithm, which, in combination with the B-Tree Dissections partitioning scheme, will be referred to as MoF–BTD. Once again we want to point out that it is reasonable to expect only a limited number of mixed cells with more than three material in the whole grid. Therefore, the computational overhead, associated with the search algorithm, is unlikely to be significant. The growth of complexity can be partially compensated by the parallel implementation: once the two groups are separated, one can refine them further completely independently.

Note that the B-Tree Dissections partitioning scheme does not make much sense in the VoF context, since it just complicates the choice of the right dissection order, which is problematic even with the much simpler Serial Dissections.

The result of the B-Tree Dissections is a *polygonal B-Tree partition*. A mixed-cell partition of size M is called a *C^2-differentiable B-Tree partition*, if all the materials can be separated from the rest with $M-1$ C^2-differentiable interfaces (the separating interfaces may form junctions, but may not cross each other). If the separating interfaces are linear, then the C^2-differentiable B-Tree partition is polygonal. Serial partition is a B-Tree partition with fixed $m = 1$ (see the description of the B-Tree Dissections above).

We claim that for any C^2-differentiable B-Tree partition the MoF–BTD algorithm results in the 2nd-order accurate approximation; if the B-Tree partition is polygonal, the result is exact.

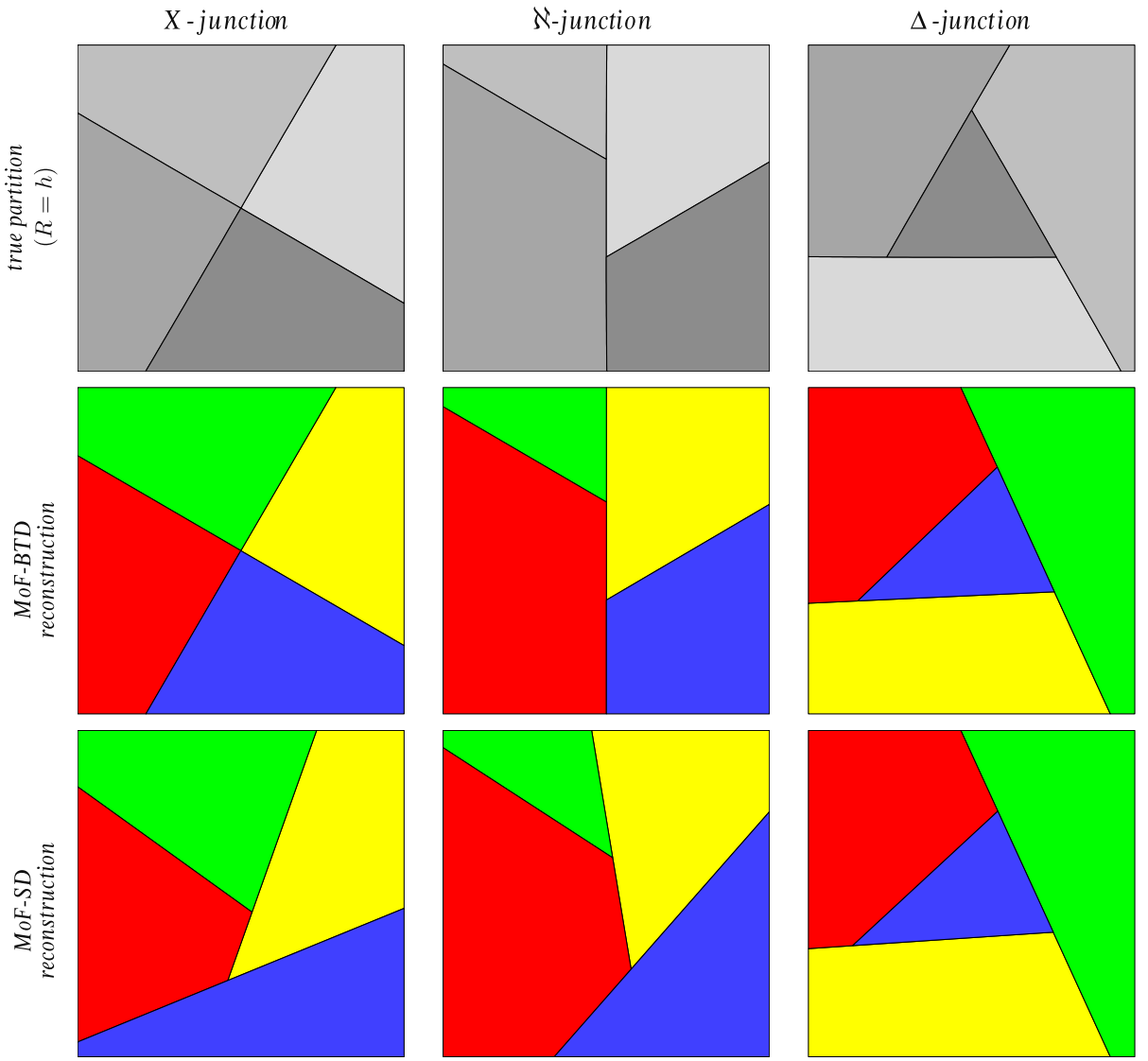

Fig. 17. The test partitions (top row, the radius of the interface curvature $R = 64h$), and their MoF reconstructions obtained with the B-Tree Dissections (middle row) and the Serial Dissections (bottom row). As the curvature of the true interfaces vanishes, the MoF–BTD reconstructions of the B-Tree layouts (the X-junction and the ℵ-junction) converge to their respective true partitions.

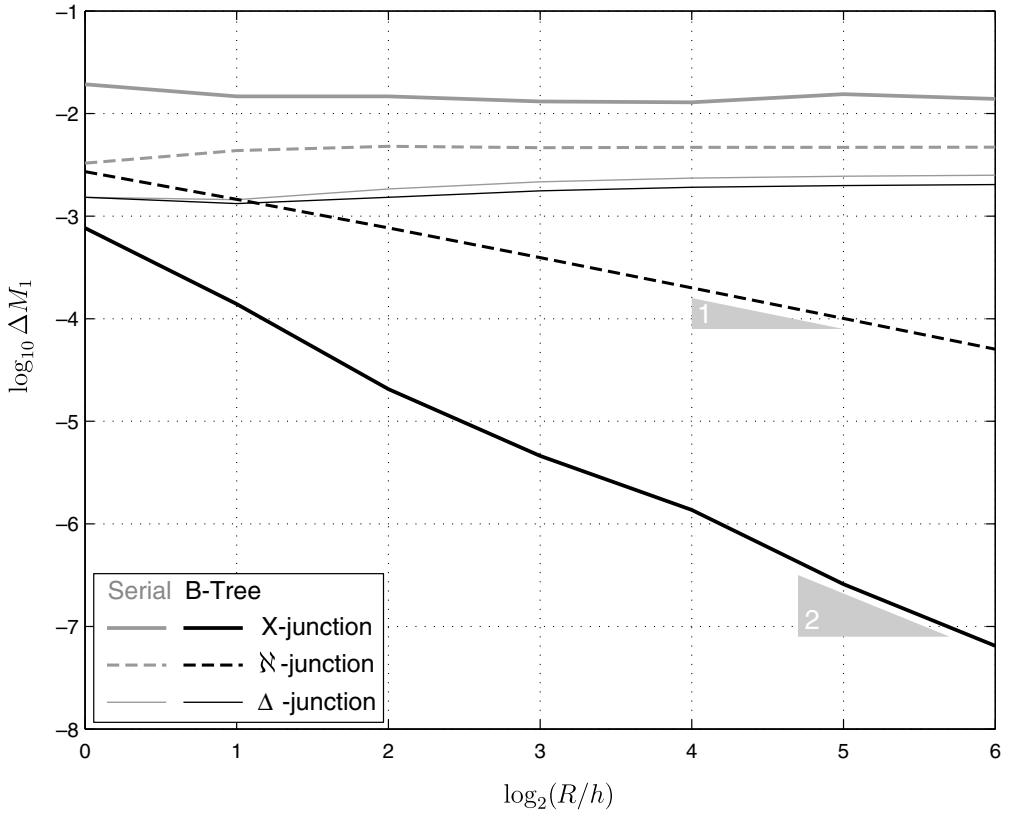

SerialDissections

$\log_2(R/h)$	ΔM_1 error		
	X-junction	ℵ-junction	Δ-junction
0	1.93e-2	3.29e-3	1.53e-3
1	1.47e-2	4.36e-3	1.45e-3
2	1.47e-2	4.78e-3	1.84e-3
3	1.31e-2	4.65e-3	2.16e-3
4	1.29e-2	4.68e-3	2.35e-3
5	1.55e-2	4.69e-3	2.45e-3
6	1.39e-2	4.70e-3	2.50e-3

B-TreeDissections

$\log_2(R/h)$	ΔM_1 error		
	X-junction	ℵ-junction	Δ-junction
0	7.64e-4	2.72e-3	1.53e-3
1	1.39e-4	1.46e-3	1.33e-3
2	2.06e-5	7.68e-4	1.53e-3
3	4.59e-6	3.94e-4	1.76e-3
4	1.37e-6	2.00e-4	1.91e-3
5	2.59e-7	1.00e-4	1.99e-3
6	6.48e-8	5.04e-5	2.03e-3

Fig. 18. The cumulative defect of the first moment ΔM_1 as a function of the interface curvature $1/R$ (the size of the mixed cell is fixed $h = 1$).

4.3.1. Numerical tests

To support our claim and compare the accuracy of the MoF–BTD reconstruction to the accuracy of the MoF–SD reconstruction, we tested three different mixed-cell layouts (see Fig. 15):

- an X-junction,
- an ℵ-junction and
- a Δ-junction.

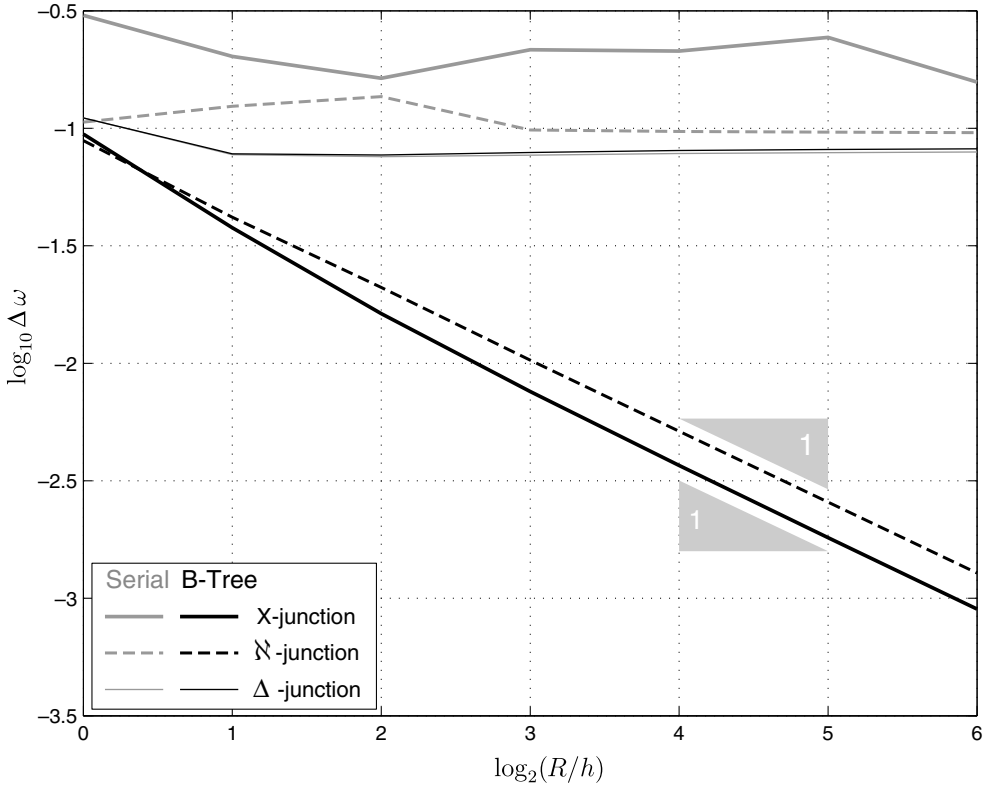

Serial Dissections

	$\Delta\omega$ error		
$\log_2(R/h)$	X-junction	ℵ-junction	Δ-junction
0	3.02e-1	1.06e-1	1.11e-1
1	2.02e-1	1.24e-1	7.73e-2
2	1.63e-1	1.36e-1	7.57e-2
3	2.16e-1	9.84e-2	7.69e-2
4	2.13e-1	9.69e-2	7.80e-2
5	2.44e-1	9.63e-2	7.88e-2
6	1.57e-1	9.59e-2	7.92e-2

B-Tree Dissections

	$\Delta\omega$ error		
$\log_2(R/h)$	X-junction	ℵ-junction	Δ-junction
0	9.49e-2	8.85e-2	1.11e-1
1	3.78e-2	4.19e-2	7.79e-2
2	1.63e-2	2.10e-2	7.70e-2
3	7.58e-3	1.03e-2	7.89e-2
4	3.68e-3	5.14e-3	8.04e-2
5	1.81e-3	2.56e-3	8.13e-2
6	8.99e-4	1.28e-3	8.18e-2

Fig. 19. The cumulative symmetric-difference area $\Delta\omega$ as a function of the interface curvature $1/R$ (the size of the mixed cell is fixed $h = 1$).

The first two configurations are C^2-differentiable B-Tree partitions, but the third one is not. Neither of the three partitions is C^2-serial. The examples of the moment-based reconstructions of these interface configurations for $R = h$ and $R = 64h$ are presented in Figs. 16 and 17, respectively.

For both algorithms we measured ΔM_1 and $\Delta\omega$ interface reconstruction errors at various Rs to build the corresponding graphs (Figs. 18 and 19, respectively). By evaluating the slopes of the $\Delta\omega$ graphs one can find that the MoF–BTD reconstruction of the X- and ℵ-junctions is 2nd-order accurate, and the MoF–BTD reconstruction of the Δ-junction is only 1st-order accurate. The Serial Dissections can not reproduce the structure of either of the test layouts and therefore their MoF–SD reconstructions are only 1st-order accurate. Table 2 summarizes the asymptotic behavior of the MoF interface reconstruction errors for all three test layouts.

Table 2
The asymptotic ($h \ll R$) behavior of the interface reconstruction errors

Error	X-junction	ℵ-junction	Δ-junction
Serial Dissections			
ΔM_1	$O(h^3)$	$O(h^3)$	$O(h^3)$
$\Delta\omega$	$O(h^2)$	$O(h^2)$	$O(h^2)$
$\Delta\Gamma$	$O(h)$	$O(h)$	$O(h)$
B-Tree Dissections			
ΔM_1	$O(h^5/R^2)$	$O(h^4/R)$	$O(h^3)$
$\Delta\omega$	$O(h^3/R)$	$O(h^3/R)$	$O(h^2)$
$\Delta\Gamma$	$O(h^2/R)$	$O(h^2/R)$	$O(h)$

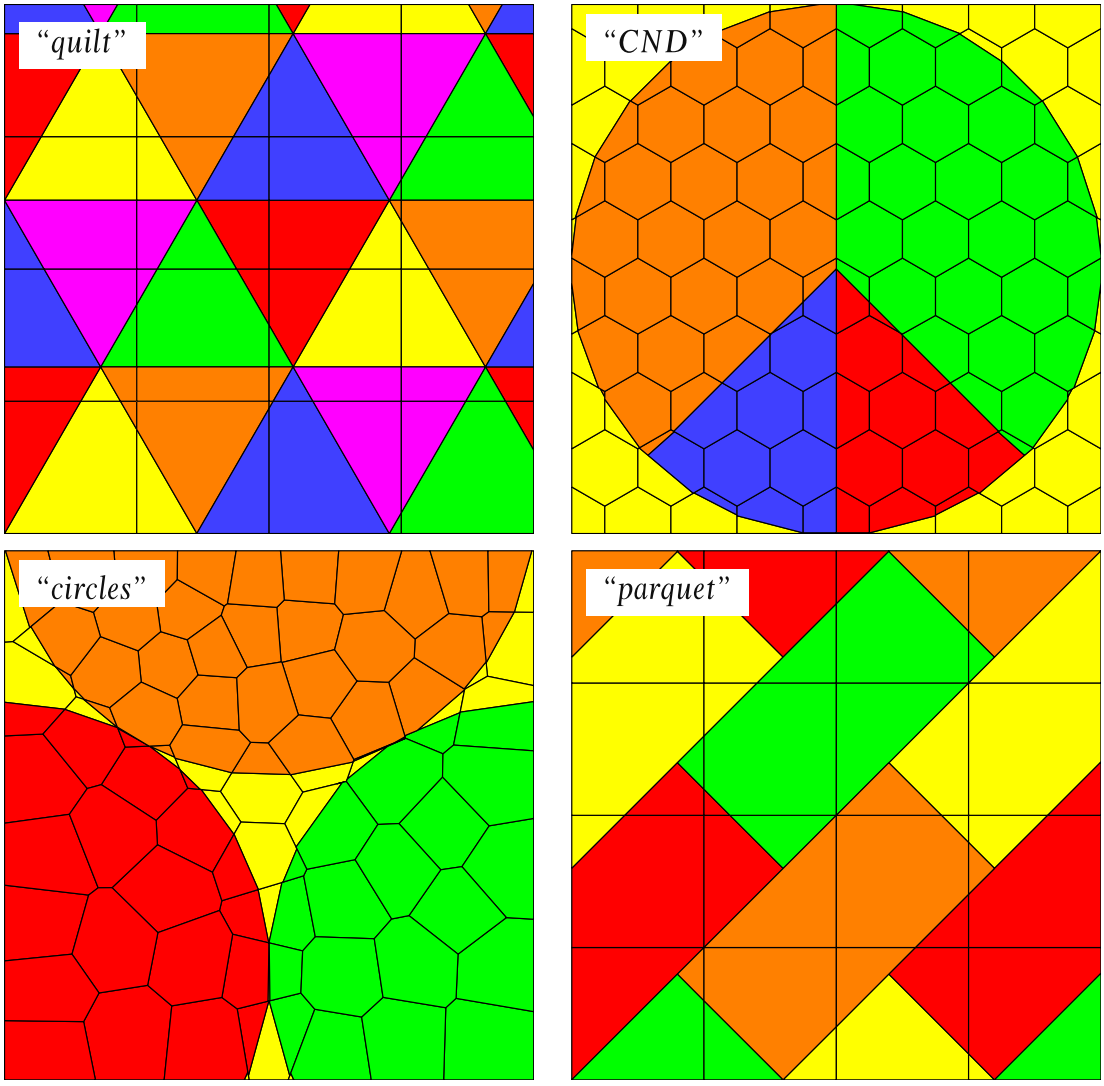

Fig. 20. These four examples demonstrate the capabilities of the multi-material MoF technique. Although the true configurations are not shown here, one can easily guess them, since their MoF reconstructions are very accurate; the "quilt" and "parquet" reconstructions are exact. The top two examples require the employment of the B-Tree Dissections, while the bottom ones can be obtained with the Serial Dissections. There is a fixed material order that can be used for "circles", but no fixed order will work for the "parquet" configuration. We would also like to emphasize the exceptional resolution of the MoF method: in case the "patchwork" and "parquet" configurations the size of the color tiles is comparable to the size of the grid cells.

At the end we would like to present four more configurations that can be accurately reproduced by the multi-material MoF algorithm (Fig. 20).

5. Concluding remarks

We reviewed the multi-material VoF interface reconstruction strategies and presented a new multi-material MoF algorithm.

Following the VoF strategy, the MoF algorithm can construct a serial mixed-cell partition by separating materials from the cell one by one. The major advantage of the MoF approach over the VoF approach is that the former provides sufficient data to choose the best approximate partition (derive the material order) automatically. Also, the multi-material MoF algorithm can go beyond the traditional serial partitions and reconstruct an arbitrary C^2-differentiable B-Tree mixed-cell partition with 2nd-order accuracy, which can hardly be achieved in the VoF context.

Although our discussion evolved around 2D cases, it is clear that all the partitioning and ordering strategies described are dimension-independent and therefore are applicable in 3D.

Acknowledgments

Authors would like to thank Blair Swartz, Rao Garimella, Rob Lowrie, Jimmy Fung, and Sam Schofield for useful discussions and valuable comments.

To create the examples presented in Fig. 20, we used the Mesh Toolkit (MSTK) library [10] developed by Rao Garimella and the Voronoï tessellation generator provided by Milan Kucharik.

Authors also acknowledge the support of the DOE Advanced Simulation and Computing (ASC) and the Laboratory Directed Research and Development (LDRD) Programs at the Los Alamos National Laboratory.

This work was carried out under the auspices of the National Nuclear Security Administration of the US Department of Energy at Los Alamos National Laboratory under Contract W-7405-ENG-36 and Contract DE-AC52-06NA25396.

Appendix A. The centroid velocity

Let ω be a parcel of incompressible fluid that moves in the velocity field $\mathbf{v}(\mathbf{x})$. Then the velocity of its centroid $\mathbf{x}_c(\omega)$ is

$$\frac{\mathrm{d}}{\mathrm{d}t}\mathbf{x}_c(\omega) = \frac{1}{|\omega|}\frac{\mathrm{d}}{\mathrm{d}t}\int_\omega \mathbf{x}\,\mathrm{d}\omega = \frac{1}{|\omega|}\int_\omega \frac{\mathrm{d}}{\mathrm{d}t}\mathbf{x}\,\mathrm{d}\omega = \frac{1}{|\omega|}\int_\omega \mathbf{v}\,\mathrm{d}\omega = \cdots$$

If the velocity field is twice-differentiable, then

$$\mathbf{v}(\mathbf{x}) = \mathbf{v}_0 + G_0(\mathbf{x}-\mathbf{x}_0) + \mathrm{O}(||\mathbf{x}-\mathbf{x}_0||^2),$$

where $\mathbf{v}_0 \equiv \mathbf{v}(\mathbf{x}_c(\omega))$ is the velocity at the parcel centroid $\mathbf{x}_0 \equiv \mathbf{x}_c(\omega)$, $G_0 \equiv [\nabla\mathbf{v}](\mathbf{x}_c(\omega))$ is the velocity gradient at the parcel centroid.

$$\begin{aligned}
\cdots &= \frac{1}{|\omega|}\int_\omega \left\{\mathbf{v}_0 + G_0(\mathbf{x}-\mathbf{x}_0) + \mathrm{O}(d^2)\right\}\mathrm{d}\omega \\
&= \frac{1}{|\omega|}\left\{\mathbf{v}_0|\omega| + G_0\left(\underbrace{\int_\omega \mathbf{x}\,\mathrm{d}\omega - \mathbf{x}_0|\omega|}_{\|\ 0}\right) + \mathrm{O}(d^2)|\omega|\right\} \\
&= \mathbf{v}_0 + \mathrm{O}(d^2),
\end{aligned}$$

where d is the diameter of the parcel $|\omega|$.

As we see, the centroid velocity coincides with the velocity at the centroid location with up to $O(d^2)$. Also, whenever $\mathbf{v}(\mathbf{x})$ is linear, the Hessian of $\mathbf{v}$ vanishes, and $O(d^2) \equiv 0$. Therefore, with high confidence, one can consider the centroid of the parcel to be a Lagrangian particle.

References

[1] D. Bailey, S. Brown, G. Zimmerman, Interface reconstruction and sub-zone physics models, Technical Report UCRL-CONF-214875, CA, 2005.

[2] David S. Bailey, Personal communications, November 2005.

[3] Timothy J. Barth, Numerical methods for gas dynamic systems on unstructured meshes, in: D. Kröner, M Ohlberger, C. Rohde (Eds.), An Introduction to Recent Developments in Theory and Numerics for Conservation Laws. Proceedings of the International School on Theory and Numerics for Conservation Laws, Freiburg/Littenweiler, October 20–24, 1997, Lecture Notes in Computational Science and Engineering, Springer-Verlag, Berlin Heidelberg, 1999, pp. 271–273.

[4] R.L. Bell, E.S. Hertel, An improved material interface reconstruction algorithm for Eulerian codes, Technical Report SAND 92-1716, Sandia National Laboratories, 1992.

[5] David J. Benson, Computational methods in Lagrangian and Eulerian hydrocodes, Computer Methods in Applied Mechanics and Engineering 99 (2–3) (1992) 235–394.

[6] David J. Benson, Eulerian finite element methods for micromechanics of heterogeneous materials: dynamic prioritization of material interfaces, Computer Methods in Applied Mechanics and Engineering 151 (3–4) (1998) 343–360.

[7] David J. Benson, Volume of fluid interface reconstruction methods for multi-material problems, Applied Mechanics Reviews 55 (2) (2002) 151–165.

[8] R. DeBar, Fundamentals of the KRAKEN code. Technical Report UCID-17366, Lawrence Livermore National Laboratory, Livermore, CA, 1974.

[9] Vadim Dyadechko, Mikhail Shashkov, Moment-of-fluid interface reconstruction. Technical Report LA-UR-05-7571, Los Alamos National Laboratory, Los Alamos, NM, October 2005. The publication is available online at <http://math.lanl.gov/~vdyadechko/doc/2007-mof.pdf>; more information on the moment-of-fluid interface reconstruction is available at <http://math.lanl.gov/~vdyadechko/research>.

[10] R.V. Garimella, MSTK: a flexible infrastructure library for developing mesh-based applications, in: Proceedings of the 13th International Meshing Roundtable, Williamsburg, VA, 2004. More information on the MSTK project is available at <http://math.lanl.gov/~rao/Meshing-Projects/MSTK>.

[11] Rao Garimella, Personal communications, November 2005.

[12] C.W. Hirt, B.D. Nichols, Volume of fluid (VOF) method for the dynamics of free boundaries, Journal of Computational Physics 39 (1) (1981) 20125.

[13] W.H. McMaster, E.Y. Gong, User's manual for pele-ic: a computer code for Eulerian hydrodynamics. Technical Report UCRL-52609, Lawrence Livermore National Laboratory, Livermore, CA, 1979.

[14] S.J. Mosso, B.K. Swartz, D.B. Kothe, R.C. Ferrell, A parallel, volume-tracking algorithm for unstructured meshes, in: P. Schiano, A. Ecer, J. Periaux, N. Satofuka (Eds.), Parallel Computational Fluid Dynamics: Algorithms and Results Using Advanced Computers, Elsevier Science, 1997, pp. 368–375.

[15] Stewart Mosso, Sean Clancy. A geometrically derived priority system for Young's interface reconstruction. Technical Report LA-CP-95-0081, Los Alamos National Laboratory, Los Alamos, NM, 1995.

[16] J.E. Pilliod, E.G. Puckett, Second-order accurate volume-of-fluid algorithms for tracking material interfaces, Journal of Computational Physics 199 (2) (2004) 465–502.

[17] E.G. Puckett, A volume-of-fluid interface tracking algorithm with applications to computing shock wave refraction. in: H. Dwyer (Ed.), Proceedings of the Fourth International Symposium on Computational Fluid Dynamics, Davis, CA, 1991, pp. 933–938.

[18] E.G. Puckett, J.S. Saltzman, A 3D adaptive mesh refinement algorithm for multimaterial gas dynamics, Physica D 60 (1–4) (1992) 84–93.

[19] William J. Rider, Douglas B. Kothe, Reconstructing volume tracking, Journal of Computational Physics 121 (2) (1998) 112–152.

[20] M. Rudman, Volume tracking methods for interfacial flow calculations, IJNMF 24 (1997) 671–691.

[21] R. Scardovelli, S. Zaleski, Direct numerical simulation of free-surface and interfacial flow, Annual Review of Fluid Mechanics 31 (1999) 567–603.

[22] Blair Swartz, The second-order sharpening of blurred smooth borders, Mathematics of Computation 52 (186) (1989) 675–714.

[23] D.L. Youngs, Time-dependent multi-material flow with large fluid distortion, in: K.W. Morton, M.J. Baines (Eds.), Numerical Methods for Fluid Dynamics, Academic Press, 1982, pp. 273–285.

[24] D.L. Youngs, An interface tracking method for a 3D Eulerian hydrodynamics code. Technical Report AWRE/44/92/35, Atomic Weapon Research Establishment, Aldermaston, Berkshire, UK, April 1987.